Journal of Solid State Chemistry 184 (2011) 584–588

Contents lists available at ScienceDirect

Journal of Solid State Chemistry

journal homepage: www.elsevier.com/locate/jssc

Evidence of network demixing in GeS_2–Ga_2S_3 chalcogenide glasses: A phase transformation study

Changgui Lin [a,b,*], Laurent Calvez [b], Haizheng Tao [a], Mathieu Allix [c], Alain Moréac [d], Xianghua Zhang [b], Xiujian Zhao [a]

[a] Key Laboratory of Silicate Materials Science and Engineering (Wuhan University of Technology), Ministry of Education, Wuhan, Hubei 430070, PR China
[b] Laboratoire des Verres et Céramiques, UMR-CNRS 6226, Sciences chimiques de Rennes, Université de Rennes 1, 35042 Rennes Cedex, France
[c] CNRS, UPR3079 CEMHTI, 45071 Orléans Cedex 2, France
[d] GMCM, UMR-CNRS 6626, Université de Rennes 1, 35042 Rennes Cedex, France

ARTICLE INFO

Article history:
Received 6 August 2010
Received in revised form
8 January 2011
Accepted 16 January 2011
Available online 25 January 2011

Keywords:
Phase transformation
Chalcogenide glass
Random network model
XRD
Thermodymanic

ABSTRACT

The information of phase transformation is attained by *in situ* XRD experiments leading to the knowledge of topological threshold in GeS_2–Ga_2S_3 glasses. The turning point of phase transformation behavior is demonstrated to be glasses containing 14–15 mol% Ga_2S_3. To interpret it a network demixing model is further improved and proposed for the structure of these ternary or quasi-binary chalcogenide glasses. For the nearest-neighbor coordination environment of glass with a transitional composition of 85.7 mol% (6/7) $GeS_2 \cdot 14.3$ mol% (1/7) Ga_2S_3, six-coordinated [S_3Ga–X–GaS_3] units (X=S or None) are well isolated by the [GeS_4] structures, which contributes to the decreasing of precipitation of Ga_2S_3 crystals in $(100-x)GeS_2$–xGa_2S_3 ($x \leq 14.3$) glasses corresponding to the experimental evidence of the phase transformation behavior. This scenario of intermediate-range structural order, firstly, includes the arrangement of structural units which is consistent with and provides an atomistic explanation of the compositional evolution of phase transformation behavior in these glasses.

1. Introduction

The residual structural order in chalcogenide glasses has continually attracted considerable interest in the past several decades, which is of crucial importance for understanding their unique physico-chemical properties, such as photoinduced phenomena. With the knowledge of random network model [1] and medium-range structural order (MRO) in covalent glasses [2], intensive investigations have been done on specific structural models in some simple binary glasses of Ge–X, Si–X, and As–X (X=S or Se) systems by experimental structural probes and computer simulation [2–10]. Since then, much effort also has been devoted to address the nature of intermediate-range order in some ternary or quasi-binary glasses, however, structural studies of these systems, e.g. GeS_2–Ga_2S_3, were inevitably limited to short-range order (SRO) scale (<0.5 nm) [11–22].

GeS_2–Ga_2S_3 chalcogenide glasses have shown many advantages for potential applications of optical modulator or frequency converter, efficient laser host materials, and fiber-optical amplifier in the IR spectral region, *e.g.* their preferable chemical and thermal stabilities, wide transparency window (up to 12 μm), low phonon energy ($\sim 340\ cm^{-1}$), and high refractive index (>2.0), etc. In particular, their rare-earth ions (REI) solubility is greatly increased through the incorporation of gallium, which acts as a network co-former and makes some structural modifications of the GeS_2 network. Intensive investigation into the structure of these glasses has been carried out [11–22], and reveals the structural dependence of the increased REI solubility [14]. The network of GeS_2–Ga_2S_3 glasses has been commonly described by various structural units and their types of interconnection (corner- or edge-shared) that was established by Raman scattering, infrared spectroscopy, and high-energy particle (X-ray or neutron) technique [11–22], etc. In spite of the existence of controversial description of the glass network in the GeS_2–Ga_2S_3 system, it is now more acceptable that the glass structure is mainly built up by corner- or edge-shared [Ge(Ga)S_4] tetrahedra and ethane-like [S_3Ga–GaS_3] units connected by bridging sulfur [12,14,20]. Unfortunately, this structural information was restricted within the SRO length scale, and no specific structural order beyond the next nearest-neighbor units was clarified. In addition, although many works deal with the crystallization of chalcogenide or chalcohalide glasses containing Ge and Ga [23–25], the crystallization mechanism was still not explained yet.

This study demonstrated the first attempt of a specific arrangement of structural units with a large atomic scale

* Corresponding author at: Key Laboratory of Silicate Materials Science and Engineering (Wuhan University of Technology), Ministry of Education, Wuhan, Hubei 430070, PR China.
E-mail addresses: linchanggui@gmail.com (C. Lin), laurent.calvez@univ-rennes1.fr (L. Calvez), opluse@whut.edu.cn (X. Zhao).

0022-4596/$ - see front matter © 2011 Elsevier Inc. All rights reserved.
doi:10.1016/j.jssc.2011.01.018

(medium-range order) through comprehensive knowledge of the topological threshold of phase transformation in GeS_2–Ga_2S_3 glasses. Hereinafter, systematical investigation of the Ga_2S_3 effect on phase transformation is performed in detail to clarify their crystallization mechanism, and further yields valuable information about the evolution of network connectivity and network topological thresholds. The resultant thermodynamic information gives a clue to optimize the usual random network model of ternary or quasi-binary glasses and to achieve a new and reasonable image of an MRO microstructure in the GeS_2–Ga_2S_3 system.

2. Experimental

Glasses with stoichiometric compositions of $(100-x)GeS_2$–xGa_2S_3 were prepared by the melt-quenching technique, where x=0, 5, 10, 14, 15, 16, 17, 19, 20, 25, and 30 mol% (delegated by Gx), respectively. Details of the glass preparation can be found elsewhere [23]. The compositions of the prepared glass was analyzed by electron probing micro-analysis (EPMA, JXA-8800R), revealing that the difference between theoretical and real compositions was within a reasonable range (± 1 at%).

To realize the crystallization behavior of GeS_2–Ga_2S_3 glasses, *in situ* XRD experiments were conducted using a conventional θ–θ Bragg-Brentano configuration (Ni-filtered Cu$K\alpha_{1,2}$=1.5418 Å) on a Bruker-AXS D8 Advance diffractometer fitted with a linear Vantec-1 detector and equipped with an Anton Paar oven chamber (model HTK 1200N), able to reach temperatures of up to 1200 °C. The calorimetric measurements were carried out using DSC (TA Q20 Thermal Analysis) at a heating rate of 10 °C/min with a temperature accuracy of ± 1 °C. Raman spectroscopy was conducted at room temperature using the back (180°) scattering configuration by the inVia Laser Confocal Raman Spectrometer (Type: Renishaw RM-1000), using a diode laser with wavelength of 785 nm. The resolution of the frequencies was ± 1 cm^{-1}.

3. Results and discussion

Fig. 1(a) and (b) present the *in situ* XRD patterns of G20 and G10 bulk glasses collected each hour (1 h scans) at 470 and 480 °C, respectively. A two-step crystallization mechanism can be clearly identified from the XRD patterns of G20 glass in Fig. 1(a). Firstly, XRD peaks ascribed to Ga_2S_3 crystals arise from the broad base profile of amorphous state; and then after about 5 h heat-treatments, GeS_2 crystal phase starts to be separated out from the residual glass matrix. It is in accordance with our previous study [23] that the Ga_2S_3 phase is precipitated prior to the GeS_2 phase resulting in an exotherm of the first (low-temperature) crystallization peak (CP) as shown in the DSC curve of G20 glass in Fig. 2, and the second (high-temperature) CP is originated from the subsequent crystallization of the GeS_2 phase. Distinct from the crystallization behavior of G20 glass, as indicated in Fig. 1(b), only GeS_2 crystallites were separated out during the heat-treatments at 480 °C from 0 to 30 h. Consequently, we can conclude that the precipitation of GeS_2 phase should be responsible for the sole CP in the DSC curve of G10 glass as shown in Fig. 2.

With the knowledge of attribution of CPs in DSC curves and crystallization behavior of G20 and G10 glasses, phase transformation in GeS_2–Ga_2S_3 glasses can be roughly revealed according to the DSC curves as shown in Fig. 2. The CPs in DSC curves are evolved from sole peak to well-separated two peaks along with the compositional change from G10 to G30, indicating their possible progress of phase transformation behavior similar to that between G20 and G10 glasses. Accordingly, a future focus will be to figure out which composition is the transitional point of

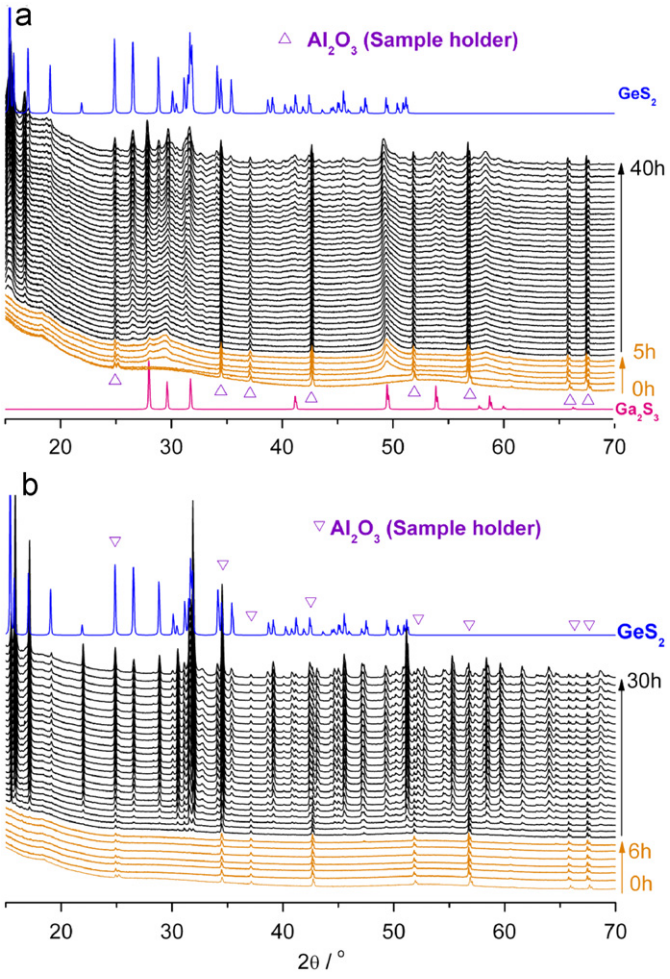

Fig. 1. *In situ* X-ray diffraction patterns of (a) G20 glass recorded every hour from 0 to 40 h at 470 °C (1 h scans), and (b) G10 one recorded every hour from 0 to 30 h at 480 °C. Alumina was used as the sample holder.

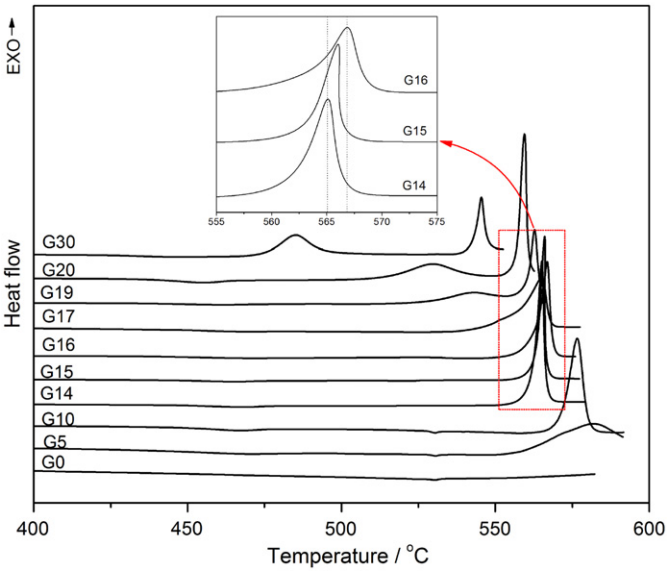

Fig. 2. DSC curves for the GeS_2–Ga_2S_3 bulk glasses at a heating rate of 10 °C/min. The detail of crystallization peaks of G14, G15, and G16 glasses is shown in the *inset*.

the distinct crystallization behavior in GeS_2–Ga_2S_3 glasses. As indicated in the inset of Fig. 2, the exothermal profiles of G16, G15, and G14 glasses are traced to the tendency to evolve from

sole CP in G14 glass to the compound CPs (two peaks) in G16 glass within a small compositional variation (only 2 mol% Ga_2S_3), suggesting conceivable distinct phase transformation behavior among these three glassy samples. Therefore, G16, G15, and G14 glasses were specially selected to obtain the specific information of the phase transformation and the possible network topological thresholds in GeS_2–Ga_2S_3 glasses.

Fig. 3 shows a set of XRD patterns of G16, G15, and G14 glasses recorded every 2 h at different temperatures. The turning point of phase transformation behavior is observable. To begin with, it is immediately clear from results of Fig. 3(a) that the crystallization behavior of G16 glass closely resembles that of G20 one. During the first 6–10 h heat-treatments, diffraction peak, located at $2\theta = 49.5^\circ$, appears and grows, suggesting that Ga_2S_3 crystals are preferentially precipitated. Subsequently, GeS_2 crystallites are identified as a new phase to present (located at $2\theta = 15.4^\circ$ and 26.4°), confirming a strong crystallization of the residual glass matrix after the 12 h heat-treatments at 470 °C. Unlike G16 glass, as displayed in Fig. 3(b), it is evident that GeS_2 and Ga_2S_3 crystal phases are formed almost at the same time (after ~12 h heat treatment) in G15 glass, leading to the simultaneous protuberance of diffraction peaks located at 15.4° and 49.5° that are ascribed to GeS_2 and Ga_2S_3 crystal phases, respectively. Surprisingly for G14 glass, despite only a very small compositional variation (1 or 2 mol% Ga_2S_3), the sequence of phase transformation is completely changed. Contrary to that of G16 and G20 glasses, the time-consuming XRD patterns of G14 glass clearly show peaks at 15.4° and 26.4° that correspond to the GeS_2 crystal phase, prior to the appearance of that of Ga_2S_3. Hence, it is easy to extract the compositional threshold of phase transformation from the above diffraction data, which is located between 14 and 15 mol% Ga_2S_3 content in GeS_2–Ga_2S_3 glasses. Noticeably, this threshold information is extremely important for us to model a more specific and reasonable atomic ordering on an intermediate length scale of 5–20 Å.

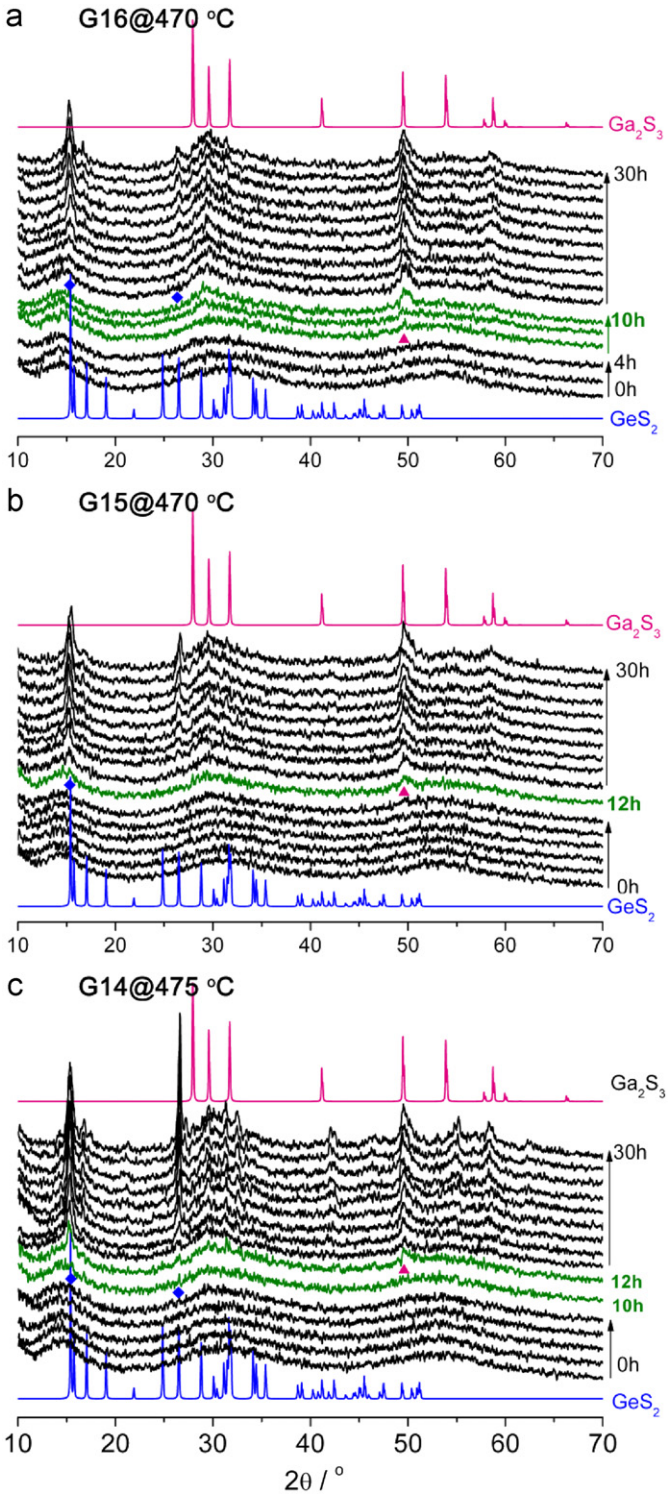

Fig. 3. XRD patterns of (a) G16, (b) G15, and (c) G14 glasses recorded every 2 h from 0 to 30 h at different temperatures, respectively.

Before structural explanation of the experimental results of phase transformation, the possible "blocks" used to construct the MRO microstructure, such as [Ge(Ga)S_4] and [S_3Ge(Ga)–Ge(Ga)S_3] structural units, should be clearly defined. However, the type of metal–metal bonds (Ge–Ge, Ge–Ga, or Ga–Ga) was still controversial in the previous literatures [11–22]. The present Raman scattering spectra, recorded in Fig. 4, would contribute to clear confusion. Different from the vibrational band of Ge–Ge located at 257 cm^{-1} in the S-deficient glass of $GeS_{1.8}$ [7,26,27], only the Raman peak of 267 cm^{-1} which was ascribed to the vibration of Ga–Ga bonds [20], and no Ge–Ge related bands are observed in the Ga_2S_3 doped glasses. Additionally, the main Raman peak at 345 cm^{-1} corresponding to [GeS_4] unit shifts immediately to 342 cm^{-1} with the addition of Ga_2S_3, indicating the formation of [GaS_4] structural units [12,14,20]. Therefore, these simple well-defined molecular-like units (e.g. ethane-like [S_3Ga–GaS_3] and [Ge(Ga)S_4] tetrahedra) would be employed as basic blocks in the next challenge to

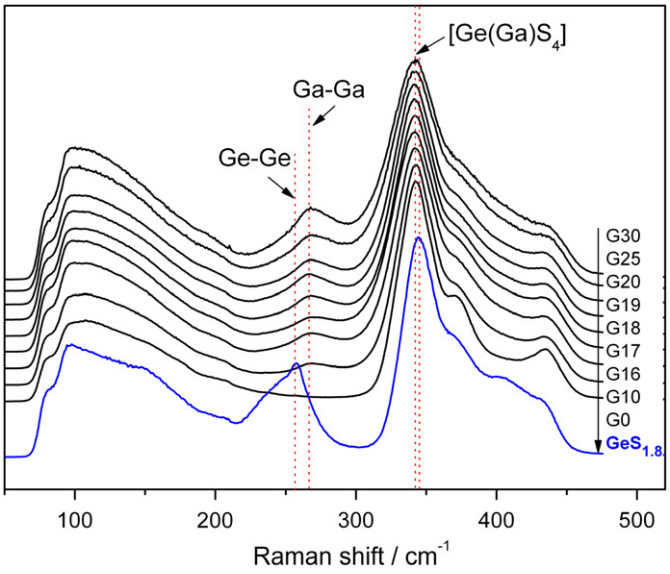

Fig. 4. Raman scattering spectra of $GeS_{1.8}$ glass and glasses of GeS_2–Ga_2S_3 system.

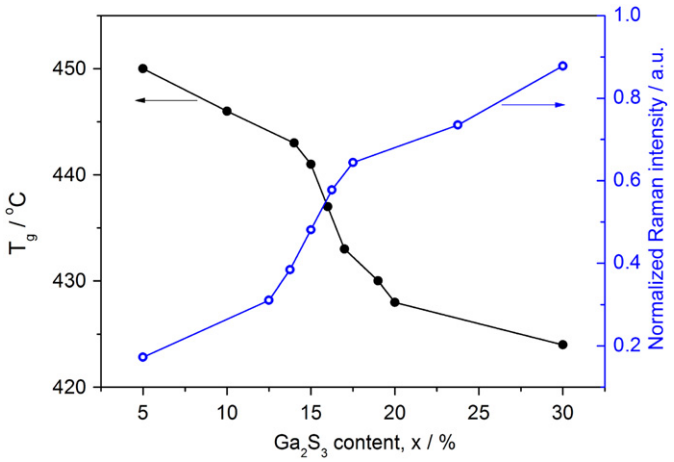

Fig. 5. Compositional trend of T_g and normalized Raman intensity at 267 cm^{-1} in GeS_2–Ga_2S_3 glasses plotted as a function of Ga_2S_3 content, x, respectively.

construct a more specific random network model and to explain the compositional evolution of phase transformation.

To begin with, the information of connectivity of GeS_2–Ga_2S_3 glass network is essential to construct their topological structure of intermediate-range order, and some evidences can be derived from Fig. 5. There is an inverse trend for the glass transition temperature T_g and normalized Raman intensity at 267 cm^{-1} of GeS_2–Ga_2S_3 glasses as the increasing of Ga_2S_3 content, x. Generally, T_g is mainly related to the energy required to break and re-form covalent bonds in a random network lattice. The weaker Ga–S bonds forming at the expense of stronger Ge–S ones determine the lowering of T_g as shown in Fig. 5. However, it is noticeable that the T_g does not linearly vary with the increase of Ga_2S_3 content, and the slop of dT_g/dx increases rapidly from 0.8 to 4 when x especially near 15% of the Ga_2S_3 content. Thus, we can realize clearly that another factor of network connectivity also influence the behavior of T_g strongly. According to the intense investigation of structural dependence on physicochemical properties conducted by Boolchand et al. [3,28–30], in this case, the loss of network connectivity, e.g. network demixing into nano-phases, is considered to be responsible for the drastical change of compositional trends in T_g. Also as displayed in Fig. 5, the Raman scattering data further nicely corroborate the above analysis. It is indicated that the network demixing of nano-phases is originated from the precipitous growth of Ga–Ga bonds, which projects as the rapid increase of Raman scattering intensity located at 267 cm^{-1}. Consequently, combined with results shown in Fig. 3, it is reasonable to deduce that once these nano-phases demixed from the network backbone, i.e. for $x > 15\%$, Ga-related crystal nuclei would be firstly nucleated in these glasses. Then, let us now consider structural dependence on phase transformation of the Ga_2S_3 modified glasses. From this point on, it is acceptable to assume that no Ga_2S_3 crystals would be precipitated if the number of nearest-neighbor structural units containing Ga is forced down into two in the local structural arrangements of GeS_2–Ga_2S_3 glasses. Based on the cognition of the existence of ethane-like [S_3Ga–GaS_3] and [GaS_4] tetrahedral units and nano-phases containing Ga–Ga bonds in the glass network, [S_3Ga–X–GaS_3] units (X=S or none) are specified to present the possible nearest-neighbor configuration of Ga-related units. Defining the six-coordinated [S_3Ga–X–GaS_3] unit as A, and the [GeS_4] one as B, it is then interesting to note that, for one A as shown in Fig. 6, six B are necessary to separate well and to prevent it from possibly linking other Ga-related ones. According to the assumption, when $A{:}B \leq 1{:}6$, the separation of Ga_2S_3 phase is restrained because the nearest-neighbor Ga-related units are equal to or less than 2 as shown in Fig. 6. In contrast, it is preferential to be

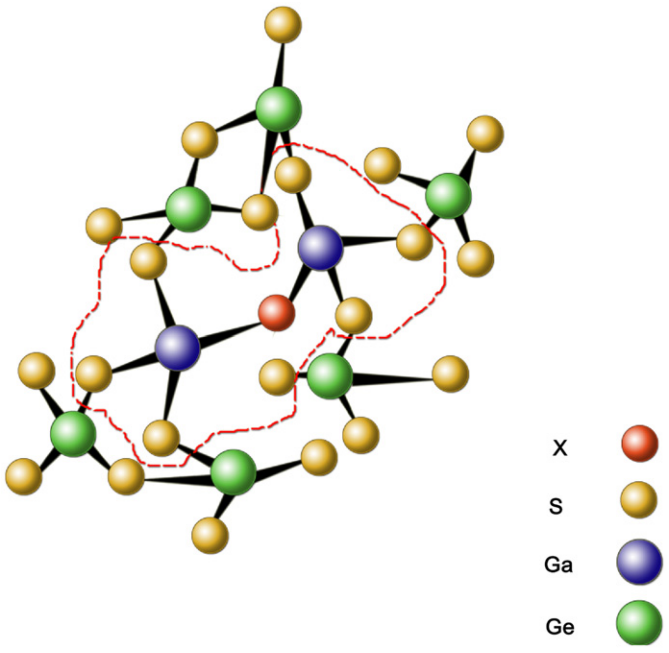

Fig. 6. Schematic representation showing the MRO structure of glass with a transitional composition at 85.7 mol% (6/7) $GeS_2 \cdot 14.3$ mol% (1/7) Ga_2S_3. X delegates the existence of S or none.

precipitated when $A{:}B > 1{:}6$. More importantly, in this model, the topological threshold is situated at the composition of 85.7 mol% (6/7) $GeS_2 \cdot 14.3$ mol% (1/7) Ga_2S_3, which is in a surprising agreement with above experimental evidences. Therefore, a new and more specific topological arrangement of the structural units is firstly proposed with an intermediate length scale for GeS_2–Ga_2S_3 glasses, which is distinguished from the traditional model that the glass structure is built up by well-defined molecular-like units connected together in a random manner.

4. Conclusions

The topological threshold of phase transformation located at 14–15 mol% Ga_2S_3 content was realized in accordance to the direct evidence of *in situ* XRD experiments. Combined with DSC curves and Raman scattering spectra, these results allowed us to construct a novel stochastic random network model, which can associate with and explain the topological threshold of phase transformation behavior and structural information reciprocally. In this model, for glasses that GeS_2 firstly precipitated ($x \leq 14.3$ mol%), the number of the nearest-neighbor units containing Ga is restricted into two maximum, i.e. [S_3Ga–X–GaS_3] units (X=S or None) are well separated by [GeS_4] tetrahedral to prevent them from bonding with other ones. The transition of phase transformation happens exactly at the glass composition of 85.7 mol% (6/7) $GeS_2 \cdot 14.3$ mol% (1/7) Ga_2S_3, consistent with the experimental results (14–15 mol% Ga_2S_3 content). It is the first structural model for the ternary or quasi-binary glass system covering the arrangement of structural units with a large atomic scale. We also should note that this process creates a new way to determine compositions with or without alkali halide, leading potentially to controllable and reproducible glass-ceramics containing nanosize particles.

Acknowledgments

This work was partially funded by the Natural Science Foundation of China (NSFC) (51032005, 60808024, 610111302140),

and the Fundamental Research Funds for the Central Universities (Wuhan University of Technology).

References

[1] Y.T. Cheng, W.L. Johnson, Science 235 (1987) 997.
[2] S.R. Elliott, Nature 354 (1991) 445.
[3] P. Boolchand, P. Chen, U. Vempati, J. Non-Cryst. Solids 355 (2009) 1773.
[4] B. Bureau, J. Troles, M. LeFloch, F. Smektala, G. Silly, J. Lucas, Solid State Sci. 5 (2003) 219.
[5] S. Kozyukhin, T. Kupriyanova, A. Vargunin, Inorg. Mater. 43 (2007) 897.
[6] P. Lucas, E.A. King, O. Gulbiten, J.L. Yarger, E. Soignard, B. Bureau, Phys. Rev. B 80 (2009) 214114.
[7] G. Lucovsky, F.L. Galeener, R.C. Keezer, R.H. Geils, H.A. Six, Phys. Rev. B 10 (1974) 5134.
[8] G. Lucovsky, J.C. Phillips, J. Non-Cryst. Solids 355 (2009) 1786.
[9] S. Sugai, Phys. Rev. Lett. 57 (1986) 456.
[10] S. Sugai, Phys. Rev. B 35 (1987) 1345.
[11] C. Julien, S. Barnier, M. Massot, N. Chbani, X. Cai, A.M. Loireau-Lozac'h, M. Guittard, Mater. Sci. Eng. B—Solid 22 (1994) 191.
[12] H. Guo, Y. Zhai, H. Tao, G. Dong, X. Zhao, Mater. Sci. Eng. B—Solid 138 (2007) 235.
[13] H. Tao, X. Zhao, C. Jing, S. Liu, J. Wuhan Univ. Technol. 20 (2005) 8.
[14] J. Heo, J. Min Yoon, S.Y. Ryou, J. Non-Cryst. Solids 238 (1998) 115.
[15] Z.G. Ivanova, J. Mol. Struct. 245 (1991) 335.
[16] Y. Ledemi, S.H. Messaddeq, I. Skhripachev, S.J.L. Ribeiro, Y. Messaddeq, J. Non-Cryst. Solids 355 (2009) 1884.
[17] A.M. Loireau-Lozac'h, F. Keller-Besrest, S. Béazeth, J. Solid State Chem. 123 (1996) 60.
[18] A. Povolotskiy, T. Ivanova, A. Manshina, Y. Tver'yanovich, S.-K. Liaw, C.L. Chang, Appl. Phys. A—Mater. 96 (2009) 887.
[19] G. Saffarini, Solid State Commun. 91 (1994) 577.
[20] A. Tverjanovich, Y.S. Tveryanovich, S. Loheider, J. Non-Cryst. Solids 208 (1996) 49.
[21] X.F. Wang, S.X. Gu, J.G. Yu, X.J. Zhao, H.Z. Tao, Solid State Commun. 130 (2004) 459.
[22] X.F. Wang, X.J. Zhao, Z.W. Wang, H.T. Guo, S.X. Gu, J.G. Yu, C.L. Liu, Q.H. Gong, Mater. Sci. Eng., B—Solid 110 (2004) 38.
[23] C. Lin, L. Calvez, M. Rozé, H. Tao, X. Zhang, X. Zhao, Appl. Phys. A—Mater. 97 (2009) 713.
[24] Y. Ledemi, B. Bureau, L. Calvez, M.L. Floch, M. Rozé, C. Lin, X. Zhang, J. Phys. Chem. B 113 (2009) 14574.
[25] M. Rozé, L. Calvez, Y. Ledemi, M. Allix, G. Matzen, X. Zhang, J. Am. Ceram. Soc. 91 (2008) 3566.
[26] H. Takebe, H. Maeda, K. Morinaga, J. Non-Cryst. Solids 291 (2001) 14.
[27] L. Cai, P. Boolchand, Philos. Mag. B 82 (2002) 1649.
[28] P. Boolchand, D.G. Georgiev, T. Qu, F. Wang, L. Cai, S. Chakravarty, C. R. Chim. 5 (11) (2002) 713–724.
[29] P. Boolchand, W.J. Bresser, Philos. Mag. B 80 (10) (2000) 1757–1772.
[30] S. Mamedov, D.G. Georgiev, T. Qu, P. Boolchand, J. Phys.—Condens. Mater. 15 (31) (2003) S2397.